 https://doi.org/10.3311/PPch.42694

Periodica Polytechnica Chemical Engineering, 70(2), pp. 370–387, 2026

Structural and Performance Optimization of Polyethersulfone Membranes with Silane Coupling Agent Coated ZnO Nanoparticles for Removal of Congo Red Dye from Wastewater

Ali Shihan Dhumad[1], Behrouz Bayati[1], Ali Amer Yahya[2*], Qusay F. Alsalhy[2**]

[1] Chemical Engineering Department, Ilam University, P.O. Box 69315/516, Ilam, Iran
[2] Membrane Technology Research Unit, Chemical Engineering Department, University of Technology- Iraq, Alsinaa Street 52, Baghdad, 10066, Iraq
[*] Corresponding author, e-mail: ali.a.yahya@uotechnology.edu.iq
[**]Corresponding author, e-mail: qusay.f.abdulhameed@uotechnology.edu.iq

Received: 03 November 2025, Accepted: 13 March 2026, Published online: 27 April 2026

Abstract

The current work introduces novel nanocomposite membranes fabricated via incorporating silane-functionalized zinc oxide nanoparticles within a polyethersulfone (PES) matrix. The membranes were synthesised via the classical phase inversion technique and bulk modified with a range of ZnO nanoparticle content from 0 to 2.5 wt.%. Comprehensive analytical techniques, including Fourier-transform infrared spectroscopy, energy-dispersive X-ray spectroscopy , field emission scanning electron microscopy , contact angle measurements and evaluations of pore size and porosity, were harnessed to identify the modification impact on membrane structure and surface characteristics. Results showed that ZnO nanoparticle content has notably influenced the morphology and physicochemical characteristics of the PES membranes. Compared to the neat PES membranes, the modified membranes had a slightly denser top surface and cross-sectional structure. Membrane wetting was remarkably improved as a reduction in contact angle from 73° to 43° was achieved. Nonetheless, the nanoadditive content was critical for membrane surface characteristics by diminishing average pore size, enhancing porosity and dye rejection efficiency, where 94.4% removal of Congo red was recorded. Furthermore, pure water flux witnesses a substantial change from 29.9 to 124.2 L/m^2·h, indicating enhanced permeability. Obtained findings underscore the futuristic potential of silane-functionalized ZnO nanoparticles to comprehensively optimize the structural integrity, hydrophilicity and separation performance of PES membranes, endowing a promising approach for efficient treatment of textile wastewater streams.

Keywords

ZnO nanomaterials, Congo red, nanocomposite membrane, membrane fouling, wastewater

1 Introduction

Current approximations reported that over 25% of the world's population is expected to witness serious water shortages by the next century [1]. The discrepancy between the freshwater supply and demand has placed massive pressure on currently available water resources [2]. Mainly, this discrepancy was induced by ongoing rise in water demand due to industrial growth, population growth, escalating per capita water demand, migration to drought-prone areas and climate change [3–7]. Within the same context, wastewater discharges from industrial streams are well recognized as the primary source of contamination to our ecosystems. This could be through infiltrating of wide spectrum of illnesses and industrial contaminations into the groundwater and direct discharge into surface water bodies, and ultimately, jeopardizing the water quality [8, 9]. Among these industrial streams, the wastewater produced by the textile industry is the major contributor to the contamination of water resources. Due to the insufficient capacity of textiles to absorb synthetic dyes, the textile industry consumes a massive amount of water and generates a significant volume of excessively colored effluent. Extremely, this colored textile effluent blocks the sunlight and diminishes the photosynthetic ability of plants indeed. Ultimately, the insufficient light penetration and oxygen

Cite this article as: Dhumad, A. S., Bayati, B., Yahya, A. A., Alsalhy, Q. F. "Structural and Performance Optimization of Polyethersulfone Membranes with Silane Coupling Agent Coated ZnO Nanoparticles for Removal of Congo Red Dye from Wastewater", Periodica Polytechnica Chemical Engineering, 70(2), pp. 370–387, 2026. https://doi.org/10.3311/PPch.42694

consumption have a harmful impact on aquatic biodiversity. Nonetheless, some artificial pigments contain metals and chlorine that might be fatal to some marine animals [10]. Therefore, before being discharged, this textile effluent should be treated to ensure it meets the required water quality standards criteria, maintains human health and sustains the ecosystem.

Particularly, the textile production process comprises several critical processes, including dyeing, printing, finishing and washing, all of which generate significant amounts of wastewater having a complex nature and posing a serious threat to the environment [11]. High concentrations of organic and inorganic pollutants, like dyes, surfactants, heavy metals and suspended particles, are frequently present in textile industry wastewater. If not adequately controlled, these contaminants pose significant threats to aquatic ecosystems and human health [10, 12, 13]. The main challenges in textile wastewater treatment are the removal of dangerous compounds, removal of color, chemical oxygen demand (COD) decline and sludge control [14]. A variety of treatment methods have been devoted to diminishing the adverse environmental impacts of textile waste, which generally comprises a combination of more than one process, including biological, physical and chemical treatments, for instance, oxidation methods, activated sludge, membrane filtration and coagulation/flocculation strategies. Recent advancements in emerging technologies such as nanotechnology, electrochemical processes and artificial wetlands have also demonstrated potential in tackling the challenges associated with treating textile wastewater [15]. Limitless endeavours are directed towards enhancing current technologies to satisfy disposal or reuse criteria [16–18]. Membrane technology is among those methods that witnessed expansion in the water treatment industry during the last several decades. The advantages offered by membrane technology in the purification of water and wastewater have contributed to this growth in several industrial sectors. With the compacted design size, low energy consumption and minimal initial capital investment, membrane technology has easily split its way into wastewater treatment applications. Besides that, with limited chemical usage, promoting environmental friendly applications and guaranteeing wide spectrum separation, membrane technology has the potential to address both economic and sustainability concerns [19, 20].

Despite the advanced state of membrane technology employed in wastewater treatment applications, the practical implementation of these processes is limited by the complex nature and versatility of fouling induced by coloured wastewater. The primary limitation of membrane operations is fouling that directly influences the efficiency of membrane performance and water quality [21]. Membrane fouling is defined as the accumulation of various contaminants on the top surface or interior of a membrane [22]. Multiple factors, including surface morphology, hydrophobicity, roughness and manufacturing material, influence the tendency of a membrane to foul [22]. Parallel to that, versatile strategies have been harnessed to mitigate the impact of membrane fouling, such as improving the design of membrane modules, using physical and chemical cleaning techniques and integrating membranes into hybrid systems [23, 24]. Moreover, membrane surface modification is a thoroughly researched field for creating a self-cleaning membrane that aims to diminish the accumulation of various contaminants on the membrane surface and, thus, avoid fouling.

A wide spectrum of chemical and physical routes has been harnessed to revise the surface characteristics of membranes and bestow self-cleaning features. Membrane modification is the act of functionalizing the surface of a membrane to impart higher hydrophilicity across the entire membrane surface. A hydrophilic surface is believed to enhance the interactions between the hydrophilic surface and the hydrophobic foulants in feed components [25]. One of the demonstrated techniques to achieve the desired hydrophilic characteristics of the membrane is through incorporating additives with hydrophilic functional groups into the polymeric matrix. Various techniques have been used to accomplish this goal, including surface chemical reactions, surface grafting, surface coating and blending, among other methodologies [26–30]. Within this specific context, the emergence of nanotechnology presented a novel platform for improving the efficiency and durability of polymeric membranes [31–34]. Metallic oxide nanoparticles, for instance, zinc oxide, titania, alumina, iron oxide (FeO), silver and many others have shown considerable potential in the field of water and wastewater treatment. Apart from their hydrophilic features, these nanomaterials possess distinctive features at the nanoscale level compared to their bulk size [32, 35–37]. Notwithstanding, integration of nanomaterials into polymeric membranes could be problematic when scaling up from laboratory to industrial scale [38]. The lack of interactions between nanoparticles and organic polymers might lead to adverse effects on membrane integrity since they aggregate and leach out of the membrane during the harsh industrial operations [39, 40]. Therefore, it is crucial to optimise the design application to ensure its

long-term stability and stable performance. Incorporating highly hydrophilic functional groups onto the surface of nanomaterials before integrating them into the polymeric membrane has been suggested recently as a feasible solution to enhance the interactions with the polymer and prevent their aggregation and leaching behaviour [41].

The objective of this work was to optimize the polyethersulfone (PES) ultrafiltration membrane design and structure aiming to improve the efficiency of PES membranes for the removal of Congo red (CR) from textile industry wastewater. This was conducted through harnessing innovative ZnO nanoparticles modified with a silane coupling agent to enhance the nanoparticle-polymer interactions and compatibility. Congo Red dye has been harnessed as an organic fouling model to perform the separation potentials of fabricated nanocomposite membranes. By adjusting the concentration of ZnO nanoparticles (NPs) in the PES membrane from 0 to 2.5 wt.%, we evaluated the impact of nanoadditive content on the characteristics of the membrane. A comprehensive characterization of the nanocomposite membrane's surface, structure, and performance will be conducted via a range of analytical tools, including contact angle (CA), field emission scanning electron microscopy (FESEM), energy dispersive spectroscopy (EDX), Fourier transform infrared spectroscopy (FTIR), pore size and porosity measurements and chemical dye rejection.

2 Experimental

2.1 Materials

Polyethersulfone with molecular mass 50 kDa, harnessed as the primary polymer for membrane fabrication, was purchased from BASF Co. Ltd. (Germany). Zinc oxide NPs with particle diameters ranging from 10 to 30 nm, coated with a silane coupling agent (purity of 99%), were purchased from SkySpring Nanomaterials Inc. (USA). A polar aprotic solvent (N,N-dimethylacetamide (DMAc)) employed to dissociate the PES polymer and polyethylene glycol (PEG), as a pore-forming agent, were both supplied by Sigma-Aldrich. Congo red dye, with molecular mass 696.66 g/mol, was obtained from a local supplier. All experimental work were performed utilizing demineralized water (DI) at the University of Technology laboratories.

2.2 Nanocomposite membrane fabrication

All PES membranes, including the control and those modified with silane-functionalized ZnO NPs, were prepared using the non-induced phase separation (NIPS) technique. The preparation of the control PES membrane initiated with dissolving PES and PEG in DMAc, followed by continuous stirring at 40 °C for 24 h to ensure complete dissociation of both components. To remove air from the polymer solution, the mixture was subjected to ultrasonic degassing. The degassed solution was then spread into a film utilizing an automated thin-film applicator, with a clearance gap of 200 μm. The casting solution was then directly immersed in a coagulation bath containing tap water. After about one minute, the membrane detached from the glass substrate, indicating completion of the phase inversion process. The formed membranes are thoroughly washed to eliminate any residual DMAc before storing in DI water.

For nanocomposite membrane fabrication, an additional step was employed at the beginning: the designated amount of silane-functionalized ZnO NPs was first dispersed in DMAc and sonicated for one hour using a bath sonicator to ensure uniform nanoparticle dispersion. This precursor was then harnessed to dissolve PES and PEG. Herein, the remaining fabrication steps followed the same steps used to prepare the pristine membrane. The composition of all membranes is given in Table 1.

2.3 Membranes testing rig setup

All ultrafiltration (UF) membrane performance, including flux and solute retention evaluation measurements, were

Table 1 Composition of fabricated membranes

Membrane code	PES (wt%)	PEG (wt%)	DMAc (wt%)	ZnO
M0	16	2	82.0	0.0% (0.000 g)
M1	16	2	81.9	0.1% (0.025 g)
M2	16	2	81.7	0.3% (0.075 g)
M3	16	2	81.3	0.7% (0.175 g)
M4	16	2	81.1	0.9% (0.225 g)
M5	16	2	80.5	1.5% (0.375 g)
M6	16	2	80.0	2.0% (0.500 g)
M7	16	2	79.5	2.5% (0.625 g)

carried out in a cross-flow filtration system. The setup featured a membrane module with an active membrane area measuring 4.2 × 4.2 cm^2. The membranes were tested under mild conditions of a feed flow rate 1.4 L/min and a transmembrane pressure 1 bar. A schematic representation of the experimental configuration is depicted in Fig. 1, illustrating its key components: a 1-liter capacity feed tank, a membrane housing unit, flow meters and pressure gauges. The circulation of the feed solution through the membrane module was facilitated by a diaphragm pump, which operated at a working pressure of 689.5 kPa and delivered a flow rate of 2.7 × 10^{-5} m^3/s.

2.4 Experimental

The structure of the prepared membranes was visualized via a field emission scanning electron microscope (TESCAN Mira3, Czech Republic) to monitor the top surface and cross-sectional morphologies. Initially liquid nitrogen was used to freeze the samples, which were fractured and sputtered with a thin layer of gold prior to imaging with the microscope at 10 kV. Energy-dispersive X-ray spectroscopy (EDax, Czech Republic) attached to the FESEM was harnessed to analyse elemental composition of membranes.

The successful integration of ZnO NPs into the PES membrane matrix, along with their chemical interaction, was confirmed via utilizing FTIR. Transmittance spectra were recorded in the range 4000 to 400 cm^{-1} using a Shimadzu IRAffinity-1S spectrometer (Japan), enabling the identification of functional groups and bonding characteristics within the composite structure. Membrane samples were carefully cleaned and dried under vacuum at 60 °C for 24 h to remove any residual moisture that might interfere with the analysis. Small pieces of the dried membranes (approximately 1 × 1 cm) were placed directly on the attenuated total reflectance (ATR) crystal, and adequate pressure was applied using the pressure clamp to ensure proper contact between the sample and the crystal surface.

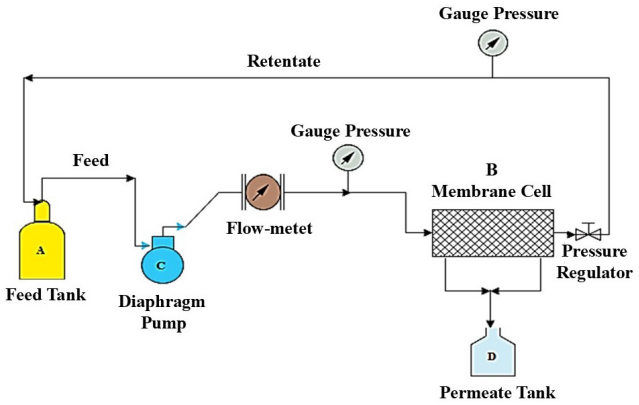

Fig. 1 Scheme of the experimental ultrafiltration system

Surface morphology and roughness of the membranes were analyzed using atomic force microscopy (AFM, model AA3000, Angstrom Advanced Inc., USA). Three-dimensional surface topography images were captured and analyzed through the AFM software, which determined the surface roughness parameters. The measurements were conducted in tapping mode over a scan area of 50 × 50 μm^2. Surface roughness parameters, including average roughness (R_a), root mean square roughness (R_q), and maximum peak-to-valley height (R_{max}) were determined from the AFM images using the instrument software.

The sessile drop method was used to measure the static contact angle between DI water and the membrane surface at room temperature using a contact angle measuring instrument (CAM 110 goniometer, Taiwan Equipment Company, Taiwan). A 3 μL droplet of deionized water was meticulously placed onto the planar membrane sample using a syringe. The contact angle between the droplet and the membrane surface was subsequently determined. Triplicate measurements were taken, and an average value was reported.

The porosity of the membranes was determined by the dry/wet method [42]. The membrane samples were cut into 3 × 3 cm^2 and soaked in DI water for an hour. The membrane surface was wiped gently to remove excessive water and weighted. After that, the samples were naturally dried at room temperature and weighted again. The porosity was measured based on the given equation below (Eq. (1)). The average of three measurements was taken.

$$\rho(\%) = \frac{\left(W_{wet} - W_{dry}\right)/D_w}{\left(W_{wet} - W_{dry}\right)/D_w + \left(W_{dry}/D_p\right)} \cdot 100\% \quad (1)$$

where ρ = membrane porosity (%), D_p = PES polymer density (1.3 g/cm^3), W_{dry} = mass of dry membrane (g), W_{wet} = mass of wet membrane (g), and D_w = water density (0.998 g/cm^3), while the mean pore radius (r_m) was estimated by the Guerout-Elford-Ferry formula below (Eq. (2)) [43]:

$$r_m = \sqrt{\frac{(2.9 - 1.75\varepsilon)8\eta \cdot l \cdot Q}{\varepsilon \cdot A \cdot \Delta P}} \quad (2)$$

where ε, η, l, Q, A, and ΔP denote the porosity, viscosity of pure water (8.9 × 10^{-4} Pa·s), thickness of membrane (m), permeate volumetric flow rate of water (m^3/s), effective membrane surface area (m^2), and operational pressure (1 bar), respectively.

The manufactured membranes were trimmed to the appropriate size, put inside the membrane unit and pressurised to 2 bar before measurements were made for the flow and rejection studies. The following Eq. (3) was used to determine the pure water flux (PWF) [44].

$$Jw = \frac{Q}{A} = \frac{V}{A \cdot t} \tag{3}$$

where J_w is the pure water flux of membrane (L/m^2·h), Q is the permeate flow rate (L/h), V is the volume of permeate (m^3), t is the permeate time (s), and A is the effective surface area of the membrane (m^2).

After the pure water experiment, the tank was drained and refilled with the 1000 mg/L Congo red solution. The performance of the membranes was evaluated based on both flux and rejection. The flux was calculated according to Eq. (3), while solute retention (R%) was based on Eq. (4) [44].

$$R(\%) = \left(\frac{C_F - C_P}{C_F} \cdot 100 \right) = \left(1 - \frac{C_P}{C_F} \right) \cdot 100, \tag{4}$$

where C_P and C_F were the concentration of solute in the permeate and the feed solutions, respectively. To determine the concentration of Congo red, the absorbance was measured by UV–Vis spectrophotometer (Chrom Tech UV-1100, E-Chrom Tech Co., Ltd., Taiwan) at 497 nm.

3 Results and discussion

3.1 Nanocomposite membranes characterization

The impact of ZnO NPs content on the nanocomposite membrane surface and cross-sectional structure was visualized via FESEM. Control PES membranes manifested a smooth surface (Fig. 2(a)), which was consistent with the typical PES membrane surface reported in literature [45]. However, all nanocomposite membranes showcased that some ZnO nanoparticles have moved close to the membrane surface during the phase separation (Figs. 2(b)-2(h)). It is noteworthy that there are slight agglomerations of nanoparticles at different locations on the nanocomposite membranes surface. The amount of big aggregates was more significant for nanocomposite membranes prepared with higher NP loading (Figs. 2(g) and 2(h)). These findings implied that the dispersion of ZnO remained advantageous when the amount of nanoparticles loading was within an optimized limit.

The cross-sectional images in Fig. 3 indicate that all synthesised membranes possess a compact, thin top layer responsible for their membrane performance, supported by a well-developed, widely porous structure. As seen, the pristine PES membrane exhibited a clear finger-like structure in the top half of the cross-section, while large macro-voids were formed in the lower half (Fig. 3(a)). This observation was induced by the rapid exchange rate between the solvent and non-solvent during the membrane formation. Meanwhile, integrating ZnO into the nanocomposite membranes induced a trivial enhancement in pore density. Besides that, the macro-void volume of each PES-ZnO membrane decreased progressively as compared to the pure PES membrane. Moreover, when the concentration of ZnO increased up to 0.5 g (Figs. 3(b)-3(f)), the membrane displayed the development of elongated and larger micropores that extended from the uppermost boundary to the lowermost boundary. This finding is consistent with the porosity data provided in preceding literature [46, 47]. Nevertheless, it is important to mention that a sponge-like structure started to emerge as the NPs concentration increased, mainly after 0.625 g of ZnO was incorporated, as the pore volume of the membrane was significantly diminished in comparison to previous PES-ZnO membranes (Fig. 3(h)). The FESEM images disclosed that the ZnO NPs at higher loadings induced higher dense membrane structure as observed. Also, a proportional rise in polymeric solution viscosity with increasing ZnO loading was evident. Consequently, the changes in porosity and pore connectivity across the membranes had a substantial impact on the flux of water.

The elemental composition of the membrane and the effective incorporation of ZnO NPs into the membrane matrix were validated by energy-dispersive X-ray spectroscopy. The elements composing the neat PES membrane and the nanocomposite membranes modified with ZnO NPs are shown in Fig. 4. The spectra associated with the control PES membrane, shown in (Fig. 4(a)), displayed prominent peaks at 0.23, 0.51, and 2.3 keV ascribed to carbon (65.31 wt%), oxygen (17.37 wt%), and sulfur (17.31 wt%), respectively. These components are characteristic elements of pure PES membranes. However, the emergence of novel peaks around 1, 8.61, and 9.7 keV provides evidence for the existence of Zn in the membrane structure after modification [46]. Significantly, the PES membrane with 2.5% ZnO showed the greatest concentration of ZnO compared to the other samples analyzed indicating successful incorporation within the polymeric matrix even at a high loading ratio.

FTIR spectroscopy was also conducted to confirm the successful incorporation of silane-functionalized ZnO NPs into the PES membrane matrix. Fig. 5 displays the transmittance

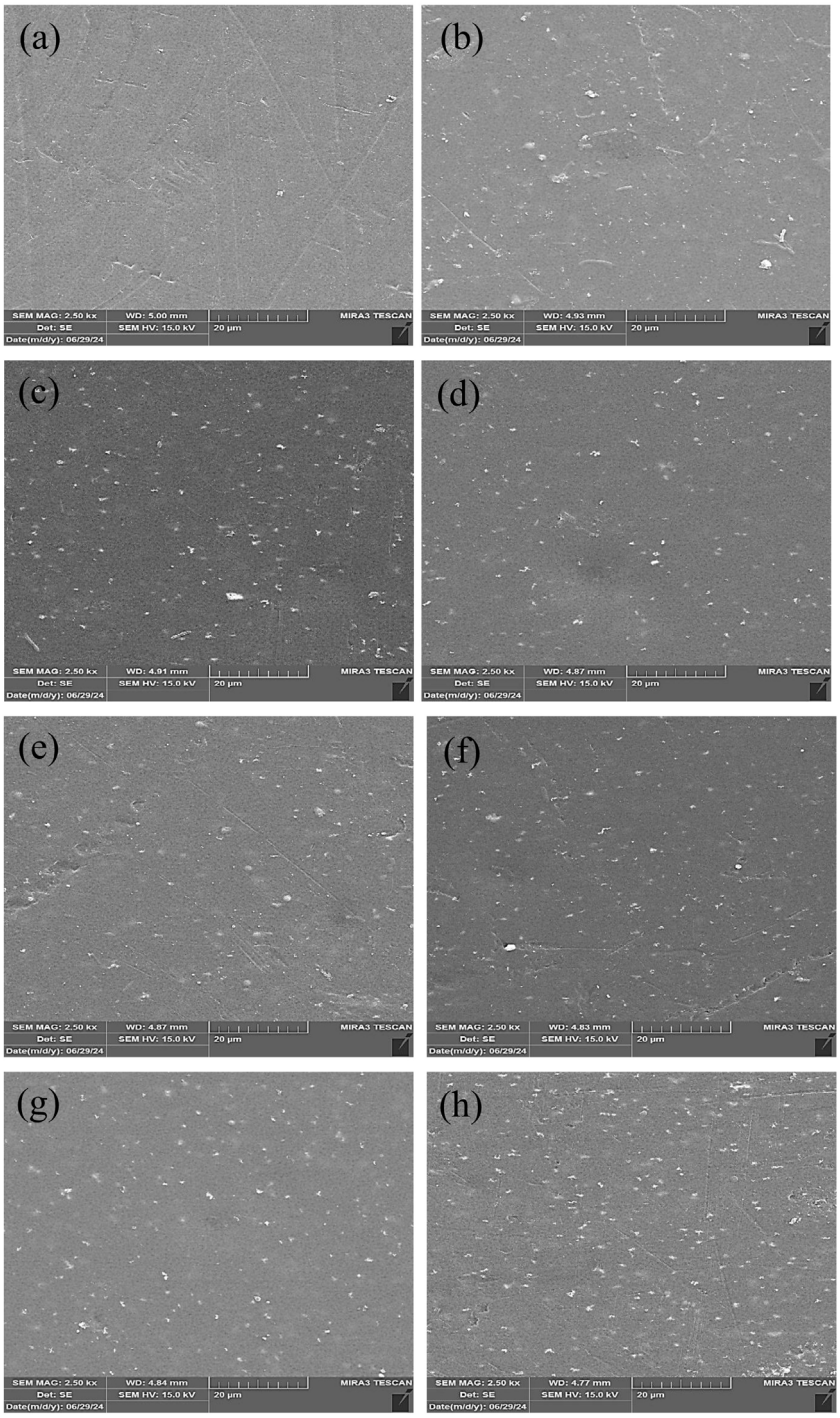

Fig. 2 FESEM surface images of PES/PEG membranes incorporated with ZnO nanoparticles at concentrations of (a) 0.0%, (b) 0.1%, (c) 0.3%, (d) 0.7%, (e) 0.9%, (f) 1.5%, (g) 2.0%, and (h) 2.5%

spectra for both neat PES and membranes modified with different ZnO concentrations (0.7% (0.175 g), 1.5% (0.375 g), and 2.5% (0.625 g)). The pristine PES membrane manifested several characteristic peaks, including aromatic C=C stretching (~1580 cm^{-1}), sulfone group vibrations (~1300 and ~1150 cm^{-1}), and ether linkages (~1100 cm^{-1}). Notably, the peaks at 1485 cm^{-1} and 1580 cm^{-1} are major characteristic peaks of the PES membrane material as reported by literature [48]. With the addition of ZnO nanoparticles, a new absorption band appeared around 400–600 cm^{-1}, corresponding to Zn−O stretching vibrations [46, 49, 50]. This peak became more intense with increasing ZnO content, confirming progressive nanoadditives incorporation. Observing minor shifts in the −OH and carbonyl regions (around 3400 cm^{-1} and 1700 cm^{-1}) further indicates possible hydrogen bonding or weak interactions between ZnO and

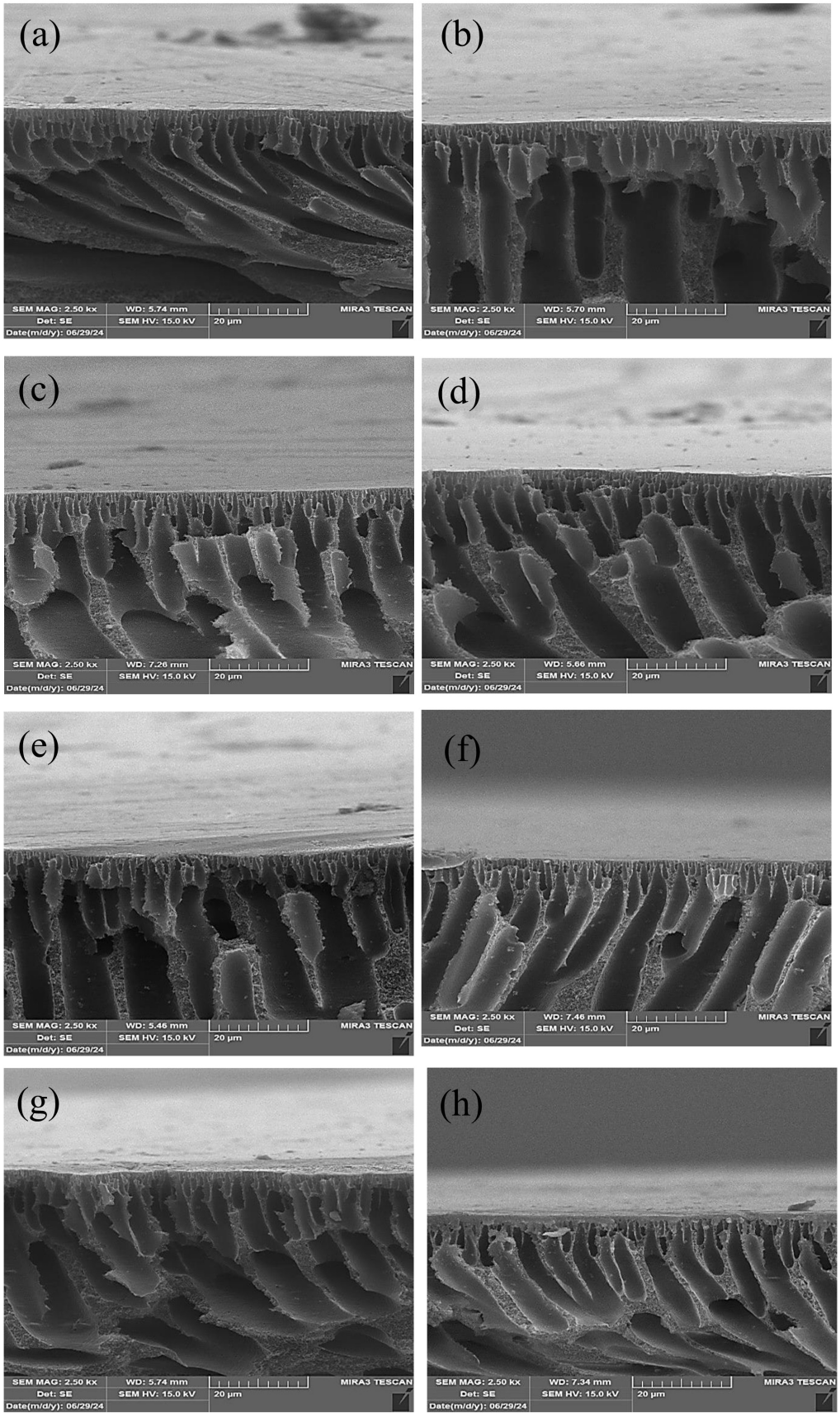

Fig. 3 FESEM cross-section images of PES/PEG membranes incorporated with ZnO nanoparticles at concentrations of (a) 0.0%, (b) 0.1%, (c) 0.3%, (d) 0.7%, (e) 0.9%, (f) 1.5%, (g) 2.0%, and (h) 2.5%

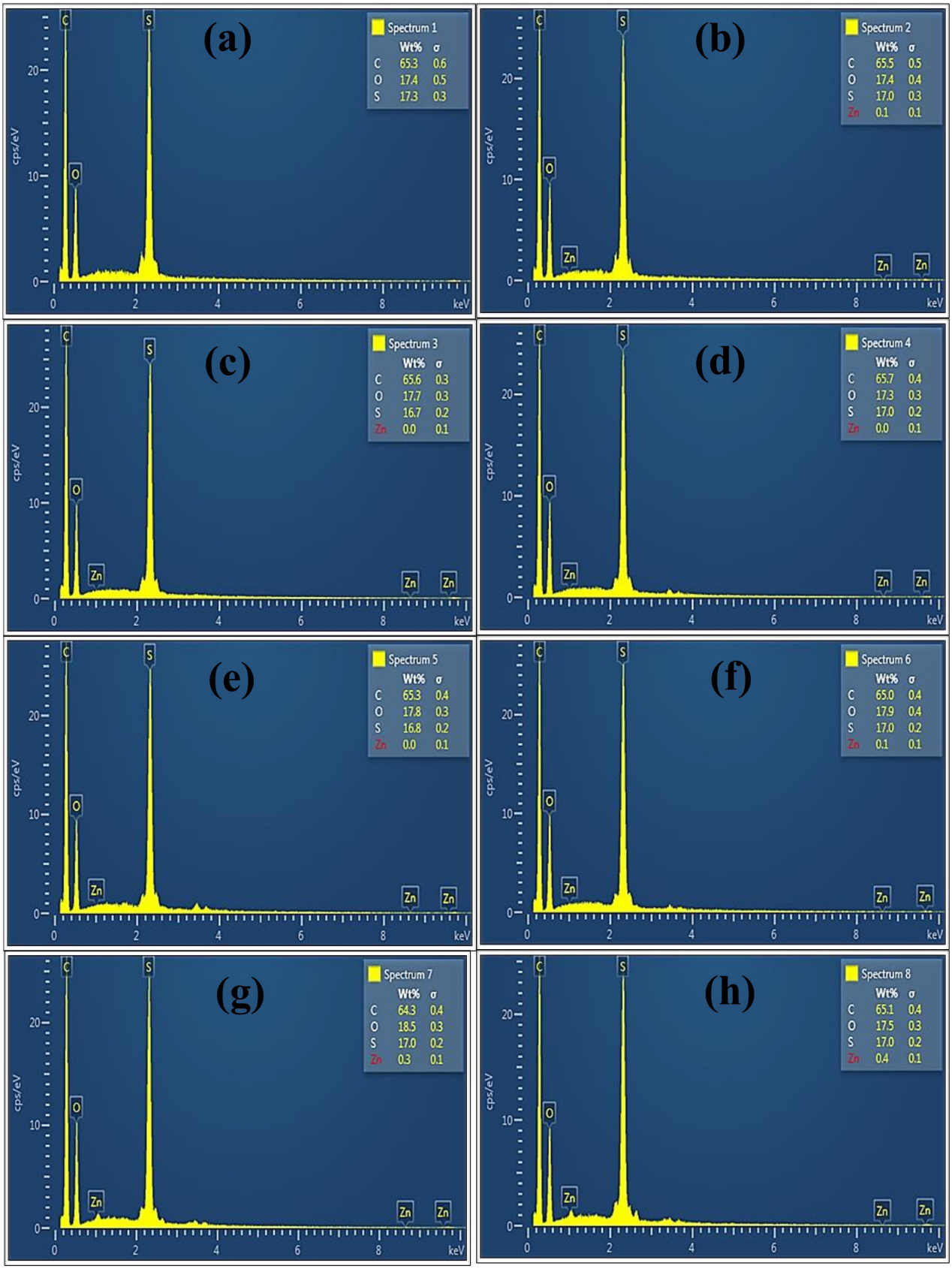

Fig. 4 EDS analysis of PES/PEG membranes incorporated with ZnO nanoparticles at concentrations of (a) 0.0%, (b) 0.1%, (c) 0.3%, (d) 0.7%, (e) 0.9%, (f) 1.5%, (g) 2.0%, and (h) 2.5%

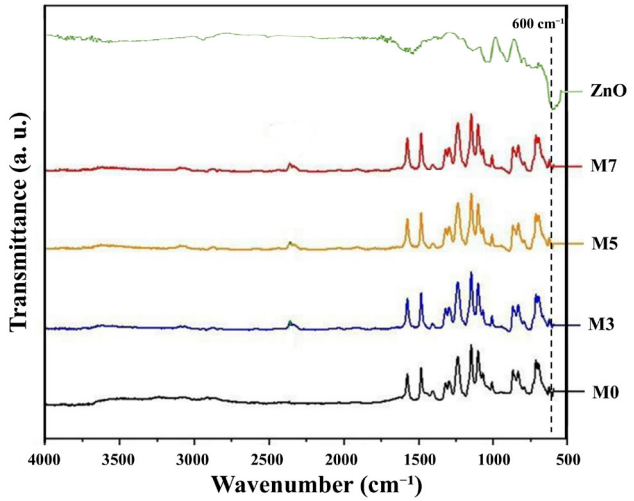

Fig. 5 FTIR spectra for unmodified and modified nanocomposite membranes identified in Table 1

the polymer matrix. These spectral modifications suggest both physical embedding and chemical interaction, contributing to enhanced surface properties [46]. In summary, the FTIR results affirm the effective integration of ZnO nanoparticles into the PES/PEG membranes, supporting observed improvements in membrane structure and performance.

Hydrophilicity is a crucial approach for predicting the permeation and antifouling properties of a membrane. Contact angle measurements have been harnessed for revealing changes in surface characteristics caused by the addition of silane-functionalized ZnO NPs. Fig. 6 presents the CA measurements for both the neat PES and ZnO-modified membrane. The unmodified PES membrane (M0) disclosed a CA value of 73°, which is within the typical range of CA associated with a neat PES membrane. Unlike all other nanocomposite membranes modified with ZnO, the neat M0 membrane exhibited the highest reported CA value. Meanwhile, this value notably decreased when ZnO was embedded into the polymeric matrix, reaching 67° when the ZnO concentration was 0.1% (M1). Incorporating additional nanoadditives resulted in a further decline in CA values, reaching 68° for M2, 65° for M3, 60° for M4, 52° for M5, and 48° for M6 nanocomposite membranes, respectively. Significantly, the M7 membrane had the lowest CA value of 43° compared to all the samples analyzed. This enhanced hydrophilicity suggests that the improved nanocomposite membrane has a stronger attraction to water. The observed change may be ascribed to the incorporation of hydrophilic functional groups or surface refinements enabled by the existence of ZnO nanoparticles. A similar observation was reported by the literature upon increasing the ZnO content in the polymeric matrix [51].

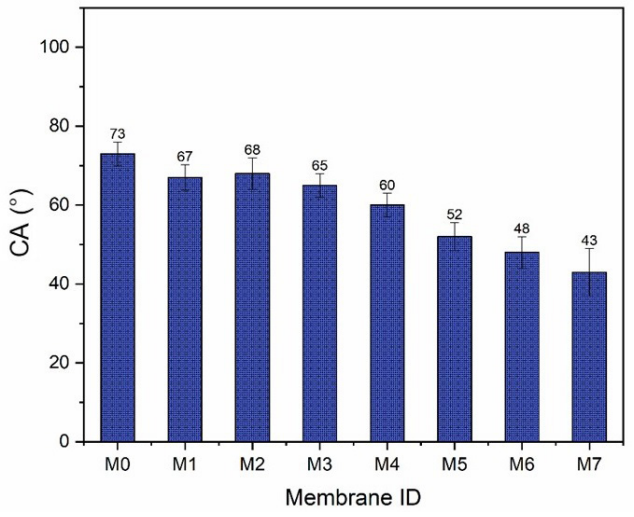

Fig. 6 Contact angle measurements of membranes identified in Table 1

The morphological surface characteristics of the fabricated PES membranes, including mean pore size, porosity, and thickness are depicted in Figs. 7(a)-7(c), respectively. As could be seen, the average pore size value displayed a noticeable decline with each amount of ZnO NPs added to the membrane matrix. Among all membranes, the pristine membrane (M0) demonstrated the highest mean pore size of 15 nm (Fig. 7(a)). As ZnO concentration increased in the nanocomposite membrane, the pore size progressively declined, reaching a minimum of 5.2 nm for M7 membrane. This reduction was mainly attributed to the increased viscosity of the casting solution and the denser membrane structure formed at high nanoadditive content [52]. The presence of ZnO likely hindered the rate of solvent–nonsolvent exchange during the phase inversion process, resulting in finer pore formation. These changes suggest a tighter membrane matrix, enhancing selectivity and mechanical integrity. In contrary to the decreasing trend observed in pore size, membrane porosity manifested an overall increase with ZnO NPs addition (Fig. 7(b)). The control PES membrane (M0) exhibited a porosityof 80%, while the nanocomposite, specifically M4 to M6, reached a peak of approximately 91–91.2%. This rise in porosity was due to the improved thermodynamic instability induced by ZnO NPs during phase separation, encouraging pore nucleation despite a reduction in their individual size [53]. The slight drop in porosity for M7 (89%) at the highest nanoadditive concentration could be result of nanoparticle agglomeration, as some pores might be blocked during the formation or even phase inversion disruption. In the meantime, membrane thickness was also measured, and it was found to fluctuate depending on the ZnO content employed to prepare the

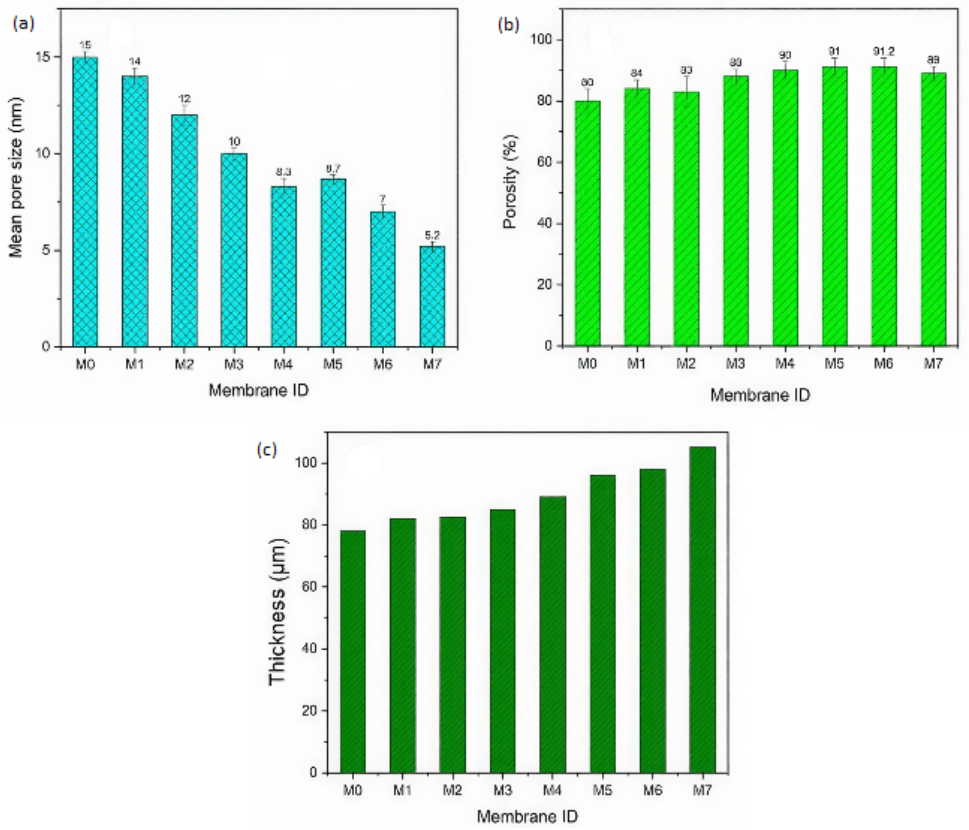

Fig. 7 Impact of nanoadditive on (a) pore size, (b) porosity and (c) thickness of fabricated membranes identified in Table 1

nanocomposite membrane (Fig. 7(c)). The pristine membrane (M0) manifested a thickness of ~78 μm, which was the lowest thickness observed amongst all modified membranes. Following the NPs addition, the membrane thickness increased proportionally with the amount of nanoadditives, recording ~83–90 μm for M1 to M4 membranes. With further ZnO loading (M5–M7), thickness increased again to ~95–105 μm, suggesting that ZnO NPs embedding has influenced the solution viscosity and film casting dynamics [54]. ZnO incorporation considerably influenced membrane surface porperties, including pore size, porosity, and thickness. The reduction in pore size coupled with increased porosity and modulated thickness implies an interplay between solution thermodynamics and kinetics during phase inversion. These structural adjustments are critical for tailoring design and performance in UF membranes for dye separation applications.

The impact of ZnO NP content on the surface topography characteristics of the fabricated membranes was assessed using AFM. Fig. 8 displays the three-dimensional topographic atomic force microscopy (AFM) images of the upper surface of the fabricated membranes. The surface roughness parameters were determined using the XEI data processing program for a 50 μm × 50 μm scan region. Control PES membranes manifested a smooth surface roughness (R_a = 12.7 nm), which is the main surface characteristic associated with PES membranes (Fig. 8(a)). Meanwhile, the relationship between the ZnO concentration used to modify the membranes and the membrane roughness parameters showed a proportional increase, as the obtained results indicated that the inclusion of ZnO leads to an increase in the roughness upon each increment in ZnO content [55]. With the incorporation of only 0.1% (M1) of the nanoadditives into the polymeric matrix, a rougher membrane surface was formed (21.9 nm) (Fig. 8(b)). Further amounts have induced more rough surfaces, reaching R_a = 30.4 and 29.7 nm for M2 and M3, respectively (Figs. 8(c) and 8(d)). The M6 and M7 membranes prepared with the highest ZnO NPs content (2.0 and 2.5%) notably exhibited a substantial escalation in the surface roughness parameter values, recording 68.8 and 131.5 nm, respectively, compared to the control PES and other modified membranes (Figs. 8(g) and 8(h)). This increase in surface roughness parameters are more likely attributed to the aggregation of ZnO on the surface of the membrane at high loading content, creating more rough surface compared to the control and lower ZnO modified membranes [56].

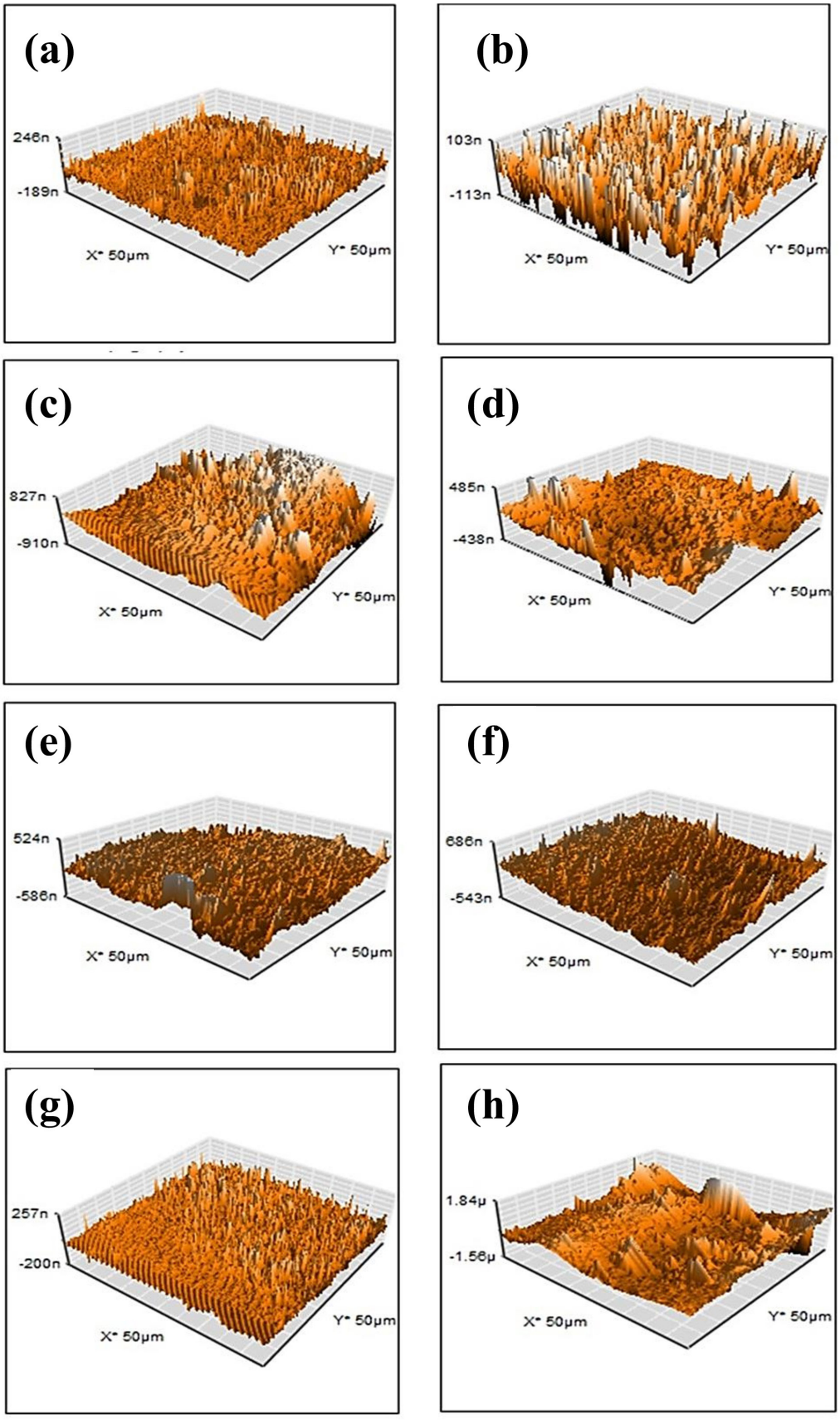

Fig. 8 Three-dimensional topographic atomic force microscopy images of PES/PEG membranes incorporated with ZnO nanoparticles at concentrations of (a) 0.0%, (b) 0.1%, (c) 0.3%, (d) 0.7%, (e) 0.9%, (f) 1.5%, (g) 2.0%, and (h) 2.5%

3.2 Performance of nanocomposite membranes modified with ZnO

In order to assess how ZnO incorporation affects solute transport behavior, the filtration performance of the fabricated membranes, both pristine and those modified with varying content of silane-functionalized ZnO NPs, was evaluated using a laboratory-scale filtration setup. The membrane flux for DI water and Congo red dye solution were measured over a 60 min filtration time, and the results are illustrated in Fig. 9. As shown, the observed permeation trend corresponds to the expected result, as explained by the improvements in hydrophilicity, pore size, and porosity previously addressed earlier in this work. The pure water flux increased markedly with each progressive increment in ZnO content in the membrane casting solution. The pristine PES membrane (M0) demonstrated the lowest water flux of 29.9 L/(m^2·h). However, with the introduction of ZnO (M1 to M7), the PWF raised steadily, reaching a peak value of 124.2 L/(m^2·h) for the M7 membrane. This increase can be attributed to several interrelated factors. Basically, this includes the witnessed improvement in hydrophilicity due to ZnO surface chemistry, which facilitates water molecule adsorption and transport [47], resulting in a dramatic reduction in the frictional resistance between the water and the pore walls and the formation of a hydration layer on the membrane surface and inside the pores [57]. This layer acts as a "lubricant," facilitating water movement and simultaneously providing resistance against foulants (antifouling), thereby sustaining a high flux [58]. Also, the enhanced surface porosity and pore interconnectivity of ZnO nanoparticles promote microphase separation during the phase inversion process [59]. To a lesser extent, the increased surface roughness effects induced by the well-dispersed nanoparticles increase the effective area available for flux. Overall, these enhancements suggest that ZnO NPs significantly optimize the membrane structure, imparting higher water permeability. The increasing PWF with ZnO loading agreed with preceding reported trends where nanomaterials act as pore formers and hydrophilic material for polymeric membrane modification [46, 60].

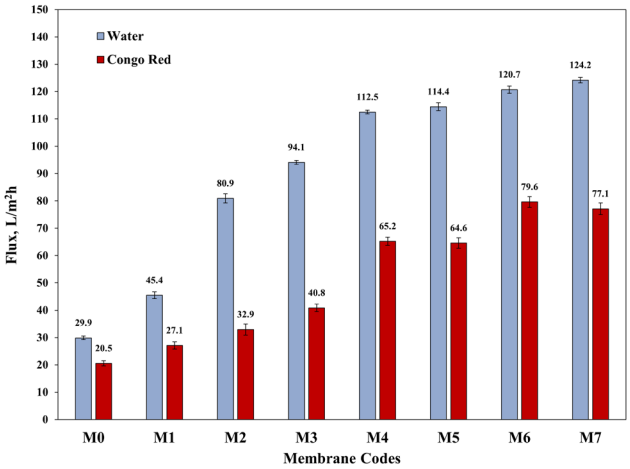

Fig. 9 Pure water flux and solute flux for nanocomposite membranes identified in Table 1

The Congo red solute flux followed a similar trend. The unmodified membrane (M0) showed a dye flux of 20.5 L/(m^2·h), which increased to a maximum of 79.6 L/(m^2·h) for membrane (M6), before showing a slight reduction to 77.1 L/(m^2·h) in membrane (M7). This performance improvement in dye permeability indicates that ZnO incorporation not only enhances water transport but also supports dye molecule diffusion through the membrane matrix, likely due to increased effective pore volume and reduced fouling tendency. However, the slight decline in flux at the highest ZnO concentration (M7) may be attributed to nanoparticle agglomeration, which can obstruct membrane pores and create localized densification in the structure. This behavior is analogous to trends observed in membranes with excessive additive loading, where solution viscosity and particle crowding disrupt optimal phase inversion [61].

The trends observed in both water and dye flux are indicative of the critical role that nanoparticle concentrations play in determining membrane morphology and filtration efficiency. Moderate ZnO content facilitates optimal membrane porosity, wettability, and structural openness, all of which enhance flux. Conversely, excessive ZnO addition may lead to nanoparticle agglomeration, increased solution viscosity, and limited phase separation, factors that can negatively impact permeability [41]. In summary, the introduction of silane-functionalized ZnO nanoparticles significantly enhances both water and solute fluxes, with optimal performance observed at intermediate to high concentrations (M4 to M6). These findings correlate well with the previously discussed surface morphology, porosity, and roughness data, confirming the beneficial influence of ZnO on membrane performance characteristics.

The Congo red rejection performance of the PES/PEG membranes modified with varying concentrations of silane-functionalized ZnO NPs is illustrated in Fig. 10, revealing a clear upward trend in dye rejection with increasing nanoparticle content. The pristine membrane (M0) exhibited the lowest rejection rate of 76.0%. As previously mentioned in this paper, this phenomenon is because of its comparatively larger pore size and decreased surface

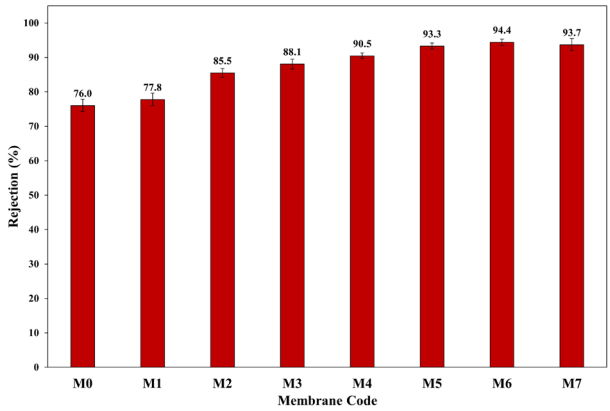

Fig. 10 Evaluation of membrane removal efficacy for Congo red. Membranes are identified in Table 1.

hydrophilicity. Wherein, as ZnO was gradually added from M1 to M6, rejection was improved significantly, reaching a maximum value of 94.4% in the M6 membrane. This enhancement can be ascribed to the structural enhancement induced by ZnO, including reduced pore size, increased surface functionality, and improved electrostatic interactions with dye molecules, all of which restrict dye permeation. Notably, M5 and M6 achieved rejection rates above 93%, indicating an optimal balance between permeability and selectivity. Although membrane M7 maintained a high rejection efficiency (93.7%), a slight decline from M6 suggests that excessive ZnO may lead to agglomeration of nanoparticles, which can introduce defects or uneven pore distribution. Overall, the results demonstrate that ZnO incorporation enhances the separation capability of PES membranes, with the most effective rejection observed at optimized nanoparticle content.

4 Membrane interaction and transport mechanisms

When PES, PEG and modified ZnO nanoparticles (with silane coupling agents) are combined in a nanocomposite membrane or adsorption system to enhance the removal of Congo red dye, several functional groups and bonding interactions play a role. These interactions primarily involve hydrogen bonding, electrostatic attraction, dipole–dipole interactions, and covalent bonding between ZnO and silane (Fig. 11). The main functional group of polyethersulfone consists of strongly polar groups such as sulfonyl ($-SO_2-$) and ether ($-O-$), which are capable of forming hydrogen bonds. In addition, there are phenyl (aromatic) rings. Despite containing polar sites that can interact with nanoparticles and polar molecules, PES is considered hydrophobic. The functional group of polyethylene glycol consists of hydroxyl ($-OH$) and ether ($-O-$) bonds. Due to its contribution to hydrogen bonding, PEGis hydrophilic and improves membrane wettability. Silane-modified zinc oxide nanoparticles contain polymer-compatible functional groups (e.g., $-CH_3$). Following hydrolysis and condensation, covalent bonds are formed between the zinc oxide and the silane. The structure of

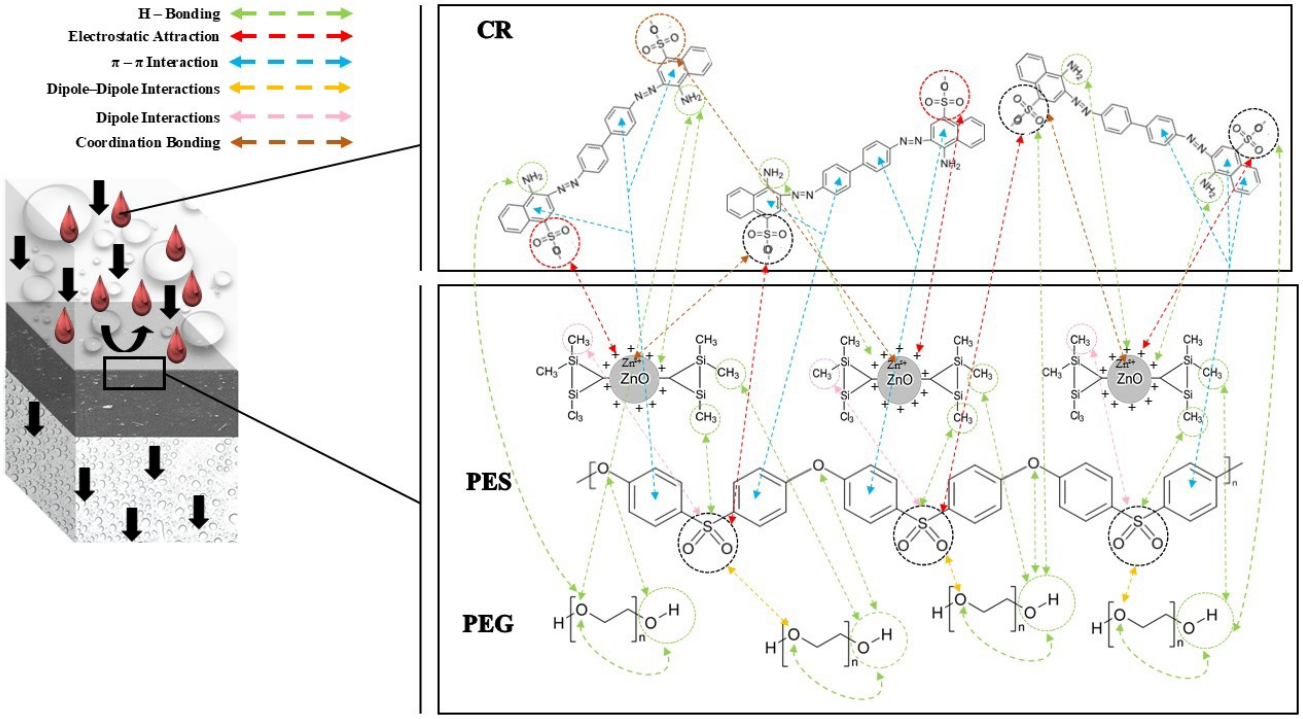

Fig. 11 Membrane interaction and transport mechanisms of PSE, PEG and ZnO (with silane) for Congo red dye removal

Congo red dye consists of azo groups (−N=N−), amino groups (−NH_2), and sulfonate groups (−SO_3^-), which are strongly negatively charged in water, and aromatic rings that enable π–π stacking with other aromatic systems. The dye is anionic in charge due to the sulfonate groups.

The interaction mechanisms between PES and PEG are characterized by hydrogen bonding, where the oxygen ether (−O−) in both PES and PEG forms hydrogen bonds with the terminal hydroxyl groups (−OH) in PEG. Dipole-dipole interactions also occur between the highly polar sulfonyl group (−SO_2−) in PES and the ether groups of PEG. PEG acts as a hydrophilic additive, increasing the hydrophilicity of the membrane surface and reducing fouling. The sulfonyl groups (−SO_2−) in PES can interact with the terminal silane groups through hydrogen bonding or dipole-dipole forces. The terminal hydroxyl groups (−OH) in PEG form hydrogen bonds with the surface hydroxyl groups of ZnO (−OH) or reactive groups on the silane (such as −CH_3). PEG helps stabilize the zinc oxide nanoparticles in the polymer matrix, preventing agglomeration. The interaction between zinc oxide (silane) and Congo red dye is also one of the strongest interactions in the system. Congo red carries negative charges (−SO_3^-) and modified zinc oxide carries positive surface charges (Zn–OH_2^+) at acidic or neutral pH, resulting in a strong electrostatic attraction. The amine (−NH_2) and sulfonate (−SO_3^-) groups in Congo red form hydrogen bonds with the silane hydroxyl groups or amine groups. Zn^{2+} ions on the ZnO surface can coordinate with the sulfonate groups in Congo red. The aromatic rings in Congo red correspond to the aromatic groups in PES, and the polar sulfonyl group (−SO_2−) in PES contains negative and positive partial dipoles, which interact with the anionic Congo red sulfonate (−SO_3^-). PEG forms hydrogen bonds between the terminal hydroxyl (−OH) or ether (−O−) groups and the sulfonate (−SO_3^-) or amino (−NH_2) groups in Congo red. This helps stabilize the adsorption of Congo red onto the membrane surface.

This complex network of interactions creates a highly efficient membrane for dye removal. PES provides structural strength, PEG provides water absorption and prevents dirt buildup, and silane-modified ZnO enhances dye capture. Congo red binds strongly to zinc oxide due to its electrostatic and coordination properties.

5 Comparison study

Table 2 presents a detailed comparison of the PES membrane developed in this study, which utilizes various pore-forming methods to create pores in PES-ZnO membranes, alongside a selection of previous studies [46, 62–68]. This table displays the key properties

Table 2 Comparison of the results observed by this work with the recent works found in the literature

Membrane composition			Application	Porosity (%)	Mean pore size (nm)	Contact angle (°)	Pure water flux (L/m²·h)	Rejection (%)	Ref.
PES polymer (wt%)	Pore former (wt%)	ZnO nanoparticle (wt%)							
16%	2% PEG	0.5%	Congo red dye removal	74	17.25	55.68	120.71	94.4%	This Work
15.75%	3.75% PVP	1.25%	Humic acid treatment	NA	72	58.1	317.45	96.12%	[62]
20%	2% PVP**	1.5%	Textile wastewater	79.5	3.98	47.9	53.3	84.1% CR; 75.6% EBT*	[46]
15%	0.85% PVP	0.0085%	Protein (BSA) separation	76.8	NA	54.8	850	97.3%	[63]
16%	4% PEG-400	0.8%	Protein (BSA) separation	78.5	NA	54.66	39	92%	[64]
16%	1% PVP	0.2%	Protein (BSA) separation	72.5	64.04	68	85.2	94.5%	[65]
17.25%	3.75% PVP	0.5%	Protein (BSA) separation	NA	3.79	57	48.05	92.30	[66]
18%	Not specified	1%	Humic acid treatment	47.34	13.96	60.9	80	94%	[67]
17%	5% PEG	1%	Wastewater rubber	73.3	NA	39.6	14.55	82%	[68]

* EBT = Eriochrome Black T dye
** PVP = Polyvinyl pyrrolidone

of the composite nanocomposite membranes, including porosity, mean pore size, contact angle, pure water flux, and solute rejection. Our PES-ZnO membranes exhibit high pure water permeability flux and solute removal efficiency, comparable to the performance of PES membranes under various conditions, as documented in previous studies.

6 Conclusions

In this work, novel nanocomposite UF membranes were successfully fabricated by incorporating different contents of silane-functionalized ZnO NPs into a PES matrix via the noninduced phase separation technique. Comprehensive characterization was conducted utilizing experimental and analytical equipment. FTIR spectroscopy confirmed the effective integration of ZnO NPs into the membrane matrix, revealing Zn−O specific absorption bands and indicative chemical interactions with the polymer backbone. Pore size analyses demonstrated that increasing ZnO NP concentration caused a significant reduction in average pore size from 15 nm in the pristine membrane to 5.2 nm in the M7 nanocomposite, while concurrently enhancing membrane porosity and surface roughness. These structural modifications translated into improved functional performance. The pure water flux increased markedly from 29.9 L/(m^2·h) for the unmodified membrane to a peak of 124.2 L/(m^2·h) at optimal ZnO loading, indicating enhanced hydrophilicity, porosity, and surface area. Similarly, Congo red dye flux and rejection efficiency followed a comparable trend, with dye rejection rising from 76.0% in the control membrane to a maximum of 94.4% in the optimally modified membrane (M6). The slight decline in performance at the highest ZnO concentration (M7) was attributed to nanoparticle agglomeration, which likely disrupted membrane uniformity and pore distribution. Overall, the findings highlight the multifunctional role of ZnO nanoparticles in simultaneously improving membrane structure, permeability, and solute rejection. Optimal nanoparticle concentrations yielded membranes with superior water flux, high dye rejection, and favorable surface characteristics, positioning ZnO-modified PES membranes as promising candidates for efficient dye-laden wastewater treatment.

References

[1] Awad, E. S., Sabirova, T. M., Tretyakova, N. A., Alsalhy, Q. F., Figoli, A., Salih, I. K. "A mini-review of enhancing ultrafiltration membranes (UF) for wastewater treatment: Performance and stability", ChemEngineering, 5(3), 34, 2021. https://doi.org/10.3390/chemengineering5030034

[2] Jackson, R. B., Carpenter, S. R., Dahm, C. N., McKnight, D. M., Naiman, R. J., Postel, S. L., Running, S. W. "Water in a changing world", Ecological Applications, 11(4), pp. 1027–1045, 2001. https://doi.org/10.1890/1051-0761(2001)011[1027:WIACW]2.0.CO;2

[3] Aljumaily, M. M., Alsaadi, M. A., Hashim, N. A., Alsalhy, Q. F., Das, R., Mjalli, F. S. "Embedded high-hydrophobic CNMs prepared by CVD technique with PVDF-co-HFP membrane for application in water desalination by DCMD", Desalination and Water Treatment, 142, pp. 37–48, 2019. https://doi.org/10.5004/dwt.2019.23431

[4] Pearce, G. K. "UF/MF pre-treatment to RO in seawater and wastewater reuse applications: a comparison of energy costs", Desalination, 222(1–3), pp. 66–73, 2008.

[5] Ghadhban, M. Y., Majdi, H. S., Rashid, K. T., Alsalhy, Q. F., Lakshmi, D. S., Salih, I. K., Figoli, A. "Removal of dye from a leather tanning factory by flat-sheet blend ultrafiltration (UF) membrane", Membranes, 10(3), 47, 2020. https://doi.org/10.3390/membranes10030047

[6] Jiang, Y. "China's water scarcity", Journal of Environmental Management, 90(11), pp. 3185–3196, 2009. https://doi.org/10.1016/j.jenvman.2009.04.016

[7] Ghadhban, M. Y., Rashid, K. T., AbdulRazak, A. A., Alsalhy, Q. F. "Recent progress and future directions of membranes green polymers for oily wastewater treatment", Water Science & Technology, 87(1), pp. 57–82, 2023. https://doi.org/10.2166/wst.2022.409

[8] Dhote, J., Ingole, S., Chavhan, A. "Review on wastewater treatment technologies", International Journal of Engineering Research & Technology, 1(5), pp. 1–10, 2012.

[9] Holkar, C. R., Jadhav, A. J., Pinjari, D. V., Mahamuni, N. M., Pandit, A. B. "A critical review on textile wastewater treatments: possible approaches", Journal of Environmental Management, 182, pp. 351–366, 2016. https://doi.org/10.1016/j.jenvman.2016.07.090

[10] Alsalhy, Q. F., Al-Ani, F. H., Al-Najar, A. E. "A new Sponge-GAC-Sponge membrane module for submerged membrane bioreactor use in hospital wastewater treatment", Biochemical Engineering Journal, 133, pp. 130–139, 2018. https://doi.org/10.1016/j.bej.2018.02.007

[11] Al-Timimi, D., Alsalhy, Q., Abdulrazak, A., Shehab, M., Nemeth, Z., Hernadi, K. "Optimum Operating Parameters for PES nanocomposite membranes for Mebeverine Hydrochloride Removal", Journal of Materials Research and Technology, 24, pp. 6779–6790, 2023. https://doi.org/10.1016/j.jmrt.2023.04.247

[12] Al-Tohamy, R., Ali, S. S., Li, F., Okasha, K. M., Mahmoud, Y. A.-G., Elsamahy, T., Jiao, H., Fu, Y., Sun, J. "A critical review on the treatment of dye-containing wastewater: Ecotoxicological and health concerns of textile dyes and possible remediation approaches for environmental safety", Ecotoxicology and Environmental Safety, 231, 113160, 2022.
https://doi.org/10.1016/j.ecoenv.2021.113160

[13] Abbas, T., Nafae, T., Alsalhy, Q., Ibrahim, Z., Al-Mashhdani, A., Al-Juboori, R. "A modified zeolite (Na2SO4 @zeolite NaA) as a novel adsorbent for radium-226,228 from acidic radioactive wastewater: Synthesis, characterization and testing", Journal of Environmental Chemical Engineering, 12(2), 112197, 2024.
https://doi.org/10.1016/j.jece.2024.112197

[14] Azanaw, A, Birlie, B., Teshome, B., Jemberie, M. "Textile effluent treatment methods and eco-friendly resolution of textile wastewater", Case Studies in Chemical and Environmental Engineering, 6, 100230, 2022.
https://doi.org/10.1016/j.cscee.2022.100230

[15] Jahan, N., Tahmid, M., Shoronika, A. Z., Fariha, A., Roy, H., Pervez, M. N., Cai, Y., Naddeo, V., Islam, M. S. "A comprehensive review on the sustainable treatment of textile wastewater: zero liquid discharge and resource recovery perspectives", Sustainability, 14(22), 15398, 2022.
https://doi.org/10.3390/su142215398

[16] Saravanan, A., Kumar, P. S., Jeevanantham, S., Karishma, S., Tajsabreen, B., Yaashikaa, P., Reshma, B. "Effective water/wastewater treatment methodologies for toxic pollutants removal: Processes and applications towards sustainable development", Chemosphere, 280, 130595, 2021.
https://doi.org/10.1016/j.chemosphere.2021.130595

[17] Abood, T. W., Shabeeb, K. M., Alzubaydi, A. B., Majdi, H. S., Al-Juboori, R. A., Alsalhy, Q. F. "Effect of MAX Phase Ti_3ALC_2 on the Ultrafiltration Membrane Properties and Performance", Membranes, 13(5), 456, 2023.
https://doi.org/10.3390/membranes13050456

[18] Abbas, T., Rashid, K., Al-Saadi, S., Alsarayreh, A. A., Figoli, A., Alsalhy, Q. "Decontamination of Aqueous Nuclear Waste via Pressure-driven Membrane Application - A Short Review", Engineering and Technology Journal, 41(9), pp. 1152–1174, 2023.
https://doi.org/10.30684/etj.2023.140193.1454

[19] Quist-Jensen, C. A., Macedonio, F., Drioli, E. "Membrane technology for water production in agriculture: Desalination and wastewater reuse", Desalination, 364, pp. 17–32, 2025.
https://doi.org/10.1016/j.desal.2015.03.001

[20] Hankins, N. P., Singh, R. "Emerging membrane technology for sustainable water treatment", Elsevier, 2016. ISBN 978-0-444-63312-5

[21] Almusawy, A., Al-Anbari, R., Alsalhy, Q. "Mitigation of membrane fouling in waste water treatment plants by using MBBR & sponge membrane bioreactor (sponge-MBR)", IOP Conference Series: Materials Science and Engineering, 1094, 012108, 2021.
https://doi.org/10.1088/1757-899X/1094/1/012108

[22] AlSawaftah, N., Abuwatfa, W., Darwish, N., Husseini, G. "A comprehensive review on membrane fouling: Mathematical modelling, prediction, diagnosis, and mitigation", Water, 13(9), 1327, 2021.
https://doi.org/10.3390/w13091327

[23] Chang, Y.-R., Lee, Y.-J., Lee, D.-J. "Membrane fouling during water or wastewater treatments: Current research updated", Journal of the Taiwan Institute of Chemical Engineers, 94, pp. 88–96, 2019.

[24] Coday, B. D., Xu, P., Beaudry, E. G., Herron, J., Lampi, K., Hancock, N. T., Cath, T. Y. "The sweet spot of forward osmosis: Treatment of produced water, drilling wastewater, and other complex and difficult liquid streams", Desalination, 333(1), pp. 23–35, 2014.
https://doi.org/10.1016/j.desal.2013.11.014

[25] Rana, D., Matsuura, T. "Surface modifications for antifouling membranes", Chemical Reviews, 110(4), pp. 2448–2471, 2010.
https://doi.org/10.1021/cr800208y

[26] Al Aani, S., Wright, C. J., Atieh, M. A., Hilal, N. "Engineering nanocomposite membranes: Addressing current challenges and future opportunities", Desalination, 401, pp. 1–15, 2017.
https://doi.org/10.1016/j.desal.2016.08.001

[27] Kadhim, R. J., Al-Ani, F. H., Alsalhy, Q. F. "MCM-41 mesoporous modified polyethersulfone nanofiltration membranes and their prospects for dyes removal", International Journal of Environmental Analytical Chemistry, 103(4), pp. 828–848, 2023.
https://doi.org/10.1080/03067319.2020.1865326

[28] Al-Araji, D. D., Al-Ani, F. H., Alsalhy, Q. F. "Modification of polyethersulfone membranes by Polyethyleneimine (PEI) grafted Silica nanoparticles and their application for textile wastewater treatment", Environmental Technology, 44(20), pp. 3033–3049, 2023.
https://doi.org/10.1080/09593330.2022.2049890

[29] Nazari, S., Abdelrasoul, A. "Impact of membrane modification and surface immobilization techniques on the hemocompatibility of hemodialysis membranes: A critical review", Membranes, 12(11), 1063, 2022.
https://doi.org/10.3390/membranes12111063

[30] Upadhyaya, L., Qian, X., Wickramasinghe, S. R. "Chemical modification of membrane surface—overview", Current Opinion in Chemical Engineering, 20, pp. 13–18, 2018.
https://doi.org/10.1016/j.coche.2018.01.002

[31] Ng, L. Y., Mohammad, A. W., Leo, C. P., Hilal, N. "Polymeric membranes incorporated with metal/metal oxide nanoparticles: A comprehensive review", Desalination, 308, pp. 15–33, 2013.
https://doi.org/10.1016/j.desal.2010.11.033

[32] Abdullah, R. R., Shabeeb, K. M., Alzubaydi, A. B., Figoli, A., Criscuoli, A., Drioli, E., Alsalhy, Q. "Characterization of the efficiency of photo-catalytic ultrafiltation PES membrane modified with tungsten oxide in the removal of tinzaparin sodium", Engineering and Technology Journal, 40(12), pp. 1633–1641, 2020.
https://doi.org/10.30684/etj.2022.134070.1219

[33] Al-Maliki, R. M., Alsalhy, Q. F., Al-Jubouri, S., Salih, I. K., AbdulRazak, A. A., Shehab, M. A., Németh, Z., Hernadi, K. "Classification of nanomaterials and the effect of graphene oxide (GO) and recently developed nanoparticles on the ultrafiltration membrane and their applications: a review", Membranes, 12(11), 1043, 2022.
https://doi.org/10.3390/membranes12111043

[34] Al-Maliki, R., Alsalhy, Q., Al-Jubouri, S., Abdulrazak, A., Shehab, M., Nemeth, Z., Hernadi, K., Majdi, H. "Enhanced Antifouling in Flat-Sheet Polyphenylsulfone Membranes Incorporating Graphene Oxide–Tungsten Oxide for Ultrafiltration Applications", Membranes, 13(3), 268, 2023. https://doi.org/10.3390/membranes13030269

[35] Al-Araji, D. D., Al-Ani, F. H., Alsalhy, Q. F. "Polyethyleneimine (PEI) grafted silica nanoparticles for polyethersulfone membranes modification and their outlooks for wastewater treatment-a review", International Journal of Environmental Analytical Chemistry, 103(16), pp. 4752–4776, 2023. https://doi.org/10.1080/03067319.2021.1931163

[36] Ali, A. M., Rashid, K. T., Yahya, A. A., Majdi, H. S., Salih, I. K., Yusoh, K., Alsalhy, Q. F., AbdulRazak, A. A., Figoli, A. "Fabrication of gum arabic-graphene (GGA) modified polyphenylsulfone (PPSU) mixed matrix membranes: A systematic evaluation study for ultrafiltration (UF) applications", Membranes, 11(7), 542, 2021. https://doi.org/10.3390/membranes11070542

[37] Kango, S., Kalia, S., Celli, A., Njuguna, J., Habibi, Y., Kumar, R. "Surface modification of inorganic nanoparticles for development of organic–inorganic nanocomposites—A review", Progress in Polymer Science, 38(8), pp. 1232–1261, 2013. https://doi.org/10.1016/j.progpolymsci.2013.02.003

[38] Ethaib, S., Al-Qutaifia, S., Al-Ansari, N., Zubaidi, S. L. "Function of nanomaterials in removing heavy metals for water and wastewater remediation: A review", Environments, 9(10), 123, 2022. https://doi.org/10.3390/environments9100123

[39] Saraswathi, M. S. S. A., Rana, D., Divya, K., Gowrishankar, S., Nagendran, A. "Versatility of hydrophilic and antifouling PVDF ultrafiltration membranes tailored with polyhexanide coated copper oxide nanoparticles", Polymer Testing, 84, 106367, 2020. https://doi.org/10.1016/j.polymertesting.2020.106367

[40] Shawket, A., Ali, N., Alsalhy, Q. "Systematic study for a comprehensive evaluation of PPSU modified with ZnO for ultrafiltration membranes: morphological characteristics and performance", Desalination and Water Treatment, 284, pp. 27–38, 2023. https://doi.org/10.5004/dwt.2023.29314

[41] Al-Araji, D., Al-Ani, F., Alsalhy, Q. "The permeation and Separation Characteristics of Polymeric Membranes Incorporated with Nanoparticles for Dye Removal and Interaction Mechanisms between Polymer and Nanoparticles: A Mini Review", Engineering and Technology Journal, 40(11), pp. 1399–1411, 2022. https://doi.org/10.30684/etj.2022.132572.1129

[42] Huang, J., Zhang, K., Wang, K., Xie, Z., Ladewig, B., Wang, H. "Fabrication of polyethersulfone-mesoporous silica nanocomposite ultrafiltration membranes with antifouling properties", Journal of Membrane Science, 423–424, pp. 362–370, 2012. https://doi.org/10.1016/j.memsci.2012.08.029

[43] Mahdi, A. E., Abbas, K. K., Aljumaily, M. M., Shaker, K. S., Wasmi, M. H., Yahya, A. A., Al-Timimi, D. A., Al-Juboori, R. A., Al-Shaeli, M., Rashid, K. T., Alsalhy, Q. F. "Preparation, characterization and applications of polyethersulfone/bentonite clay composite for protein removal", Desalination and Water Treatment, 320, 100653, 2024. https://doi.org/10.1016/j.dwt.2024.100653

[44] Goh, P. S., Lau, W. J., Othman, M. H. D., Ismail, A. F. "Membrane fouling in desalination and its mitigation strategies", Desalination, 425, pp. 130–155, 2018. https://doi.org/10.1016/j.desal.2017.10.018

[45] Al Aani, S., Wright, C. J., Hilal, N. "Investigation of UF membranes fouling and potentials as pre-treatment step in desalination and surface water applications", Desalination, 432, pp. 115–127, 2018. https://doi.org/10.1016/j.desal.2018.01.017

[46] Mezher, H. M., Adeli, H., Alsalhy, Q. F. "Novel ZnO-Modified Polyethersulfone Nanocomposite Membranes for Nanofiltration of Concentrated Textile Wastewater", Water, Air, & Soil Pollution, 235(2), 138, 2024. https://doi.org/10.1007/s11270-024-06927-7

[47] Al-Ansary, H. K., Al-Ani, F. H., Hernadi, K., Alsalhy, Q. F. "Optimization of PPSU membranes with ZnO nanoparticles: A morphological and performance evaluation", Desalination and Water Treatment, 321, 101062. https://doi.org/10.1016/j.dwt.2025.101062

[48] Al Aani, S., Haroutounian, A., Wright, C. J., Hilal, N. "Thin Film Nanocomposite (TFN) membranes modified with polydopamine coated metals/carbon-nanostructures for desalination applications", Desalination, 427, pp. 60–74, 2018. https://doi.org/10.1016/j.desal.2017.10.011

[49] Bhuyan, T., Mishra, K., Khanuja, M., Prasad, R., Varma, A. "Biosynthesis of zinc oxide nanoparticles from Azadirachta indica for antibacterial and photocatalytic applications", Materials Science in Semiconductor Processing, 32, pp. 55–61, 2015. https://doi.org/10.1016/j.mssp.2014.12.053

[50] Khan, Z. R., Khan, M. S., Zulfequar, M., Khan, M. S. "Optical and structural properties of ZnO thin films fabricated by sol-gel method", Materials Sciences and Applications, 2(5), pp. 340–345, 2011. https://doi.org/10.4236/msa.2011.25044

[51] Jo, Y. J., Choi, E. Y., Choi, N. W., Kim, C. K. "Antibacterial and hydrophilic characteristics of poly (ether sulfone) composite membranes containing zinc oxide nanoparticles grafted with hydrophilic polymers", Industrial & Engineering Chemistry Research, 55(28), pp. 7801–7809, 2016. https://doi.org/10.1021/acs.iecr.6b01510

[52] Yingyao, L., Wenxin, X., Duanchao, C., Gang, C., Qinwen, W. "Preparation of polyaniline-ZnO/PES mixed matrix membrane and its application in alkali recovery from pulping and papermaking black liquor", Environmental Progress & Sustainable Energy, 45(1), e70194, 2025. https://doi.org/10.1002/ep.70194

[53] Sotto, A., Boromand, A., Balta, S., Kim, J., Van der Bruggen, B. "Doping of polyethersulfone nanofiltration membranes: antifouling effect observed at ultralow concentrations of TiO_2 nanoparticles", Journal of Materials Chemistry, 21(28), pp. 10311–10320, 2011. https://doi.org/10.1039/C1JM11040C

[54] Rajaeian, B., Heitz, A., Tade, M. O., Liu, S. "Improved separation and antifouling performance of PVA thin film nanocomposite membranes incorporated with carboxylated TiO_2 nanoparticles", Journal of Membrane Science, 485, pp. 48–59, 2015. https://doi.org/10.1016/j.memsci.2015.03.009

[55] Balta, S., Sotto, A., Luis, P., Benea, L., Van der Bruggen, B., Kim, J. "A new outlook on membrane enhancement with nanoparticles: The alternative of ZnO", Journal of Membrane Science, 389, pp. 155–161, 2012. https://doi.org/10.1016/j.memsci.2011.10.025

[56] Rabiee, H., Farahani, M. H., Vatanpour, V. "Preparation and characterization of emulsion poly (vinyl chloride)(EPVC)/TiO_2 nanocomposite ultrafiltration membrane", Journal of Membrane Science, 472, pp. 185–193, 2014. https://doi.org/10.1016/j.memsci.2014.08.051

[57] Rabiee, H., Vatanpour, V., Farahani, M. H., Zarrabi, H. "Improvement in flux and antifouling properties of PVC ultrafiltration membranes by incorporation of zinc oxide (ZnO) nanoparticles", Separation and Purification Technology, 156, pp. 299–310, 2015. https://doi.org/10.1016/j.seppur.2015.10.015

[58] Kusworo, T. D., Aryanti, N., Dalanta, F. "Effects of incorporating ZnO on characteristic, performance, and antifouling potential of PSf membrane for PRW treatment", InIOP Conference Series: Materials Science and Engineering, 1053(1), 012134, 2021. https://doi.org/10.1088/1757-899X/1053/1/012134

[59] Acarer, S., Pir, İ., Tüfekci, M., Erkoç, T., Öztekin, V., Dikicioğlu, C., Demirkol, G. T., Durak, S. G., Özçoban, M. Ş., Çoban, T. Y., Çavuş, S. "Characterisation and mechanical modelling of polyacrylonitrile-based nanocomposite membranes reinforced with silica nanoparticles", Nanomaterials, 12(21), 3721, 2022. https://doi.org/10.3390/nano12213721

[60] Ibraheem, B. M., Al-Timimi, D. A. H., Abdullah, S. N., Majdi, H. S., Alsalhy, Q. F. "Decoration of polyethersulfone membranes with zinc oxide nanoparticles for efficient treatment of food dyes", Chemical Engineering Research and Design, 218, pp. 312–327, 2025. https://doi.org/10.1016/j.cherd.2025.05.005

[61] Saif Al Aani, V. G., Wright, C. J., Hilal, N. "Fabrication of antibacterial mixed matrix nanocomposite membranes using hybrid nanostructure of silver coated multi-walled carbon nanotubes", Chemical Engineering Journal, 326, pp. 721–736, 2017. https://doi.org/10.1016/j.cej.2017.06.029

[62] Ahmad, A. L., Abdulkarim, A. A., Ismail, S., Ooi, B. S. "Preparation and characterisation of PES-ZnO mixed matrix membranes for humic acid removal", Desalination and Water Treatment, 54(12), pp. 3257–3268, 2015. https://doi.org/10.1080/19443994.2014.91013

[63] Zhao, S., Yan, W., Shi, M., Wang, Z., Wang, J., Wang, S. "Improving permeability and antifouling performance of polyethersulfone ultrafiltration membrane by incorporation of ZnO-DMF dispersion containing nano-ZnO and polyvinylpyrrolidone", Journal of Membrane Science, 478, pp. 105–116, 2015. https://doi.org/10.1016/j.memsci.2014.12.050

[64] Shen, L., Bian, X., Lu, X., Shi, L., Liu, Z., Chen, L., Hou, Z., Fan, K. "Preparation and characterization of ZnO/polyethersulfone (PES) hybrid membranes", Desalination, 293, pp. 21–29, 2012.

[65] Ali, R. S., Hassan, A. K., Shabeeb, K. M., Al-Shaeli, M., Ladewig, B. P., Alsalhy, Q. F. "Impact of modified ZnO and evaporation time on the fabrication and performance of PES nanocomposite membranes", Desalination and Water Treatment, 322, 101190, 2025. https://doi.org/10.1016/j.dwt.2025.101190

[66] Ahmad, A. L., Abdulkarim, A. A., Shafie, Z. M., Ooi, B.S. "Fouling evaluation of PES/ZnO mixed matrix hollow fiber membrane", Desalination, 403, pp. 53–63, 2017. https://doi.org/10.1016/j.desal.2016.10.008

[67] Ahmad, A. L., Sugumaran, J., Shoparwe, N. F. "Antifouling properties of PES membranes by blending with ZnO nanoparticles and NMP–acetone mixture as solvent", Membranes, 8(4), 131, 2018. https://doi.org/10.3390/membranes8040131

[68] Kusworo, T. D., Aryanti, N., Utomo, D. P., Nurmala, E. "Performance evaluation of PES-ZnO nanohybrid using a combination of UV irradiation and cross-linking for wastewater treatment of the rubber industry to clean water", Journal of Membrane Science and Research, 7(1), pp. 4–13, 2021. https://doi.org/10.22079/JMSR.2020.120490.1334